

Spectral scaling of the aftershocks of the Tocopilla 2007 earthquake in northern Chile

M. Lancieri,^{1,2} R. Madariaga¹ and F. Bonilla²

¹Laboratoire de Géologie CNRS-Ecole Normale Supérieure, 75231 Paris Cedex 05, France. E-mail: maria.lancieri@irsn.fr

²Institut de Radioprotection et Sécurité Nucléaire, 92262 Fontenay-aux-Roses, France

Accepted 2011 December 1. Received 2011 September 15; in original form 2011 April 4

SUMMARY

We study the scaling of spectral properties of a set of 68 aftershocks of the 2007 November 14 Tocopilla (M 7.8) earthquake in northern Chile. These are all subduction events with similar reverse faulting focal mechanism that were recorded by a homogenous network of continuously recording strong motion instruments. The seismic moment and the corner frequency are obtained assuming that the aftershocks satisfy an inverse omega-square spectral decay; radiated energy is computed integrating the square velocity spectrum corrected for attenuation at high frequencies and for the finite bandwidth effect. Using a graphical approach, we test the scaling of seismic spectrum, and the scale invariance of the apparent stress drop with the earthquake size. To test whether the Tocopilla aftershocks scale with a single parameter, we introduce a non-dimensional number, $C_r = \frac{\mu E_s \beta^3}{M_0^2 f_c^3}$, that should be constant if earthquakes are self-similar. For the Tocopilla aftershocks, C_r varies by a factor of 2. More interestingly, C_r for the aftershocks is close to 2, the value that is expected for events that are approximately modelled by a circular crack. Thus, in spite of obvious differences in waveforms, the aftershocks of the Tocopilla earthquake are self-similar. The main shock is different because its records contain large near-field waves. Finally, we investigate the scaling of energy release rate, G_c , with the slip. We estimated G_c from our previous estimates of the source parameters, assuming a simple circular crack model. We find that G_c values scale with the slip, and are in good agreement with those found by Abercrombie and Rice for the Northridge aftershocks.

Key words: Earthquake dynamics; Earthquake ground motions; Earthquake source observations.

1 INTRODUCTION

The simplest, but most important property of earthquakes is the spectral scaling proposed by Aki (1967). From the study of the difference in magnitude estimations at different frequencies, he proposed that seismic moment (M_0) was inversely proportional to the cube of the corner frequency (f_c). These are essentially static parameters, related to slip and dimensions of the fault. To these parameters, it was later added the total radiated energy (E_r), a dynamic parameter that it is very difficult to estimate because of station distribution and attenuation in the earth (Brune 1970; Kanamori 1977; Boatwright 1980; Perez-Campos & Beroza 2001). From energy, we can compute the apparent stress σ_a , defined as the ratio of radiated energy to seismic moment multiplied by the rigidity (μ). Some theoretical basis for the scaling laws was found for simple source model with circular shape (Kostrov 1964; Brune 1970; Sato & Hirasawa 1973; Madariaga 1976). However, obviously a circular rupture model is not appropriate for many earthquakes. It is, thus, important to try to understand whether and why the scaling applies for earthquake in different tectonic environments.

Thanks to the development of broad-band digital seismic networks starting from the nineties, many authors have investigated self-similarity from measurements of radiated energy, corner frequency and seismic moment. Because of many practical difficulties to determine accurately these parameters, the published results are not all in agreement. Certain authors state that earthquakes follow the scaling law (Kanamori *et al.* 1993; Abercrombie 1995; Mayeda & Walter 1996; Izutani & Kanamori 2001; Prejean & Ellsworth 2001; Richardson & Jordan 2002; Mori *et al.* 2003; Stork & Ito 2004; Mayeda *et al.* 2007; Oth *et al.* 2010); others claim that earthquakes violate self-similarity (Choy & Boatwright 1995; McGarr 1999; Ide & Beroza 2001; Ide *et al.* 2003; Imanishi *et al.* 2004; Matsuzawa *et al.* 2004; Prieto *et al.* 2004; Yamada *et al.* 2005; Shearer *et al.* 2006).

In this paper, we investigate scaling relationships of the aftershocks of a M_w 7.8 subduction earthquake that occurred near the city of Tocopilla (northern Chile) on 2007 November 14. We study the main event and 68 aftershocks recorded from 2007 November 14 to 29. The Tocopilla event was a large thrust earthquake that occurred at the bottom of the interface between the Nazca and

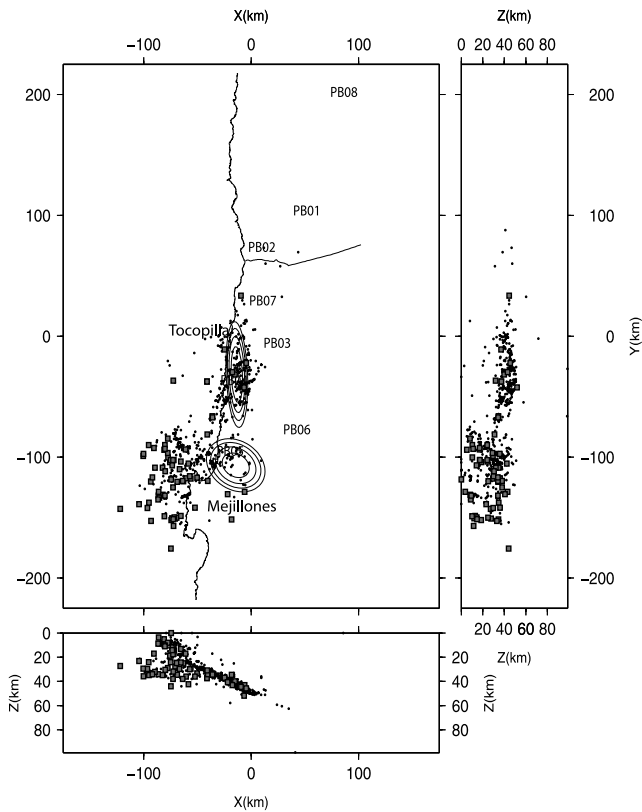


Figure 1. IPOC Network and event locations. The aftershocks that we studied ($M \geq 4$) are plotted as grey squares. The black dots are the smaller events ($M < 4$). The contour lines show the slip distribution of the main event inverted from strong motion data by (Peyrat *et al.* 2010).

South American plates, breaking a narrow (about 30–50 km) area of 130 km of length (Fig. 1; Delouis *et al.* 2009; Peyrat *et al.* 2010). Its rupture zone is contiguous with the northern bound of the area ruptured by the 1995 Antofagasta earthquake (Ruegg *et al.* 1996; Chlieh *et al.* 2004). Many reasons made this event and its aftershocks an interesting case of study. These are all subduction events with similar reverse faulting focal mechanism that were recorded by a homogenous network of continuously recording strong motion instruments. The data set covers six orders of magnitude of M_0 (10^{15} – 10^{21} Nm). Furthermore, the instruments are located in sites excavated in rock, far from any sedimentary basins. Also, as will be shown, northern Chile is a region where anelastic attenuation is weak and site effects are limited. Besides the scaling of spectra, we will also investigate the scaling of the energy release rate with the earthquake size. The energy release rate, G_c , is defined as the energy per area required to propagate the seismic rupture. In laboratory experiments (Ohnaka 2003) and in field observations (Scholz 2002), G_c scales with the event size. Many authors have measured G_c of the overall rupture process using different methods (Husseini *et al.* 1975; Das 1976; Aki 1979; Beroza & Spudich 1988; Guatteri *et al.* 2001; Ide *et al.* 2003; Mai *et al.* 2006) obtaining values ranging from 10^2 to 10^8 Jm $^{-2}$. Tinti *et al.* (2005) evaluated the breakdown work (the vectorial form of G_c) integrating the scalar product between the dynamic traction and the slip velocity over the fault plane. They observe that for earthquake having magnitude between 5.2 and 7.6, the breakdown work scales with the seismic moment. Abercrombie & Rice (2005) evaluated G_c from the source parameters estimated inverting the seismic spectrum. They found that G_c scales with slip, as predicted by the circular crack model of Madariaga (1976).

2 DATA SET

The Tocopilla data set is composed of 68 shallow thrust events with magnitudes M_w ranging from 4 to 6.8, and depth varying between 20 and 40 km. These events are the aftershocks of the Tocopilla earthquake in northern Chile. This earthquake broke the bottom of the plate interface between the Mejillones peninsula and the city of Tocopilla (Fig. 1). Two big M 6.8 aftershocks extended the rupture oceanwards from the Mejillones peninsula on 2007 November 15 (Peyrat *et al.* 2010).

The aftershocks were all recorded by the Integrated Plate boundary Observatory, Chile (IPOC) network, a permanent, continuously recording network of 17 sites covering the northern part of Chile (from Antofagasta to Arica) with a mean station spacing of 80 km (Schurr *et al.* 2009). This network was deployed by the Geoforschung Zentrum (GFZ) of Postdam, Germany and by Institut de Physique du Globe of Paris, France. All the sites are equipped with continuously recording broad-band seismometers and accelerometers. For further information on event detection and location, we refer to Lancieri *et al.* (2011). In Fig. 1, we show the location of the stations within 120 km of the area covered by the aftershocks. We also plot on this figure the aftershock distribution. The events used in this study, with $M \geq 4.0$, are reported as grey squares; most of them are located offshore the Mejillones peninsula. For each event, we use all the stations located within 110 km from the epicentre to study its spectral properties. The ellipses plotted in this figure represent the slip distribution of the main event inverted from near-source strong-motion data by Peyrat *et al.* (2010). Although this is an interesting data set for studying the scaling of seismic spectra, it suffers from poor azimuthal coverage. The largest events are all located offshore the Mejillones peninsula near the southern end of the network. This is a problem that we will always face in studying the Chilean subduction earthquakes, because these are mostly located offshore. However, we do not really expect a strong directivity effect, given that the aftershocks are almost pure thrust events and, hence, the S waves are emitted almost perpendicularly to the fault plane.

3 METHOD

We measure the M_0 , f_c and E_r from the S phase of strong motion records. To properly identify the S -phase window, we manually picked the S arrival time. We made sure that later phases did not interfere with the spectral measurements adjusting the length of the time window as a function of event magnitude. For different clusters of magnitude, we determined the window length that spanned the full S phase without including later phases using an energy criterion. Starting from the S arrival up to the end of the signal, we computed the cumulative integral of the squared velocity, and we fixed the end of the window when the integral reached 95 per cent of its final value. This operation led us to use windows whose duration ranges from 10 s for M 4 events to 50 s for the M 7.8 main event. After the signal windowing, we applied a 1 per cent cosine taper and we added zeros before and after the signal for a total duration of four times the length of the S signal. We then evaluated the fast Fourier transform on strong motion data. The velocity and displacement spectra were estimated from the Fourier acceleration spectra.

3.1 Spectral inversion technique

Determination of f_c is affected by seismic attenuation. To account for the quality factor, Q , we corrected the spectra using the method

proposed by Imanishi *et al.* (2004) and Oth *et al.* (2010). We, then, perform a two steps spectral analysis to:

1. Estimate the anelastic attenuation.
2. Compute M_0 and f_c from the displacement spectra corrected for attenuation.

Because of poor azimuthal coverage, we could not perform a joint inversion of Q and f_c as in Bonilla *et al.* (1997). We, therefore, modelled attenuation measuring the κ parameter, which controls the exponential decay of the strong motion spectrum at high frequencies (Anderson & Hough 1984),

$$a(f) = A_0 \exp(-\pi\kappa f), \quad (1)$$

where $a(f)$ is the acceleration spectrum; A_0 is the high frequency plateau and f is the frequency. In Fig. 2, we show an example of the determination of κ for the M_w 6.3 aftershock of 2007 November 15 using the three closest stations. For each station, we plot the acceleration spectrum in linear-log scale; for each component the value of κ is the slope of the linear decay measured in the 5–20 Hz range. The horizontal spectra was corrected using the average of κ on the two components, and we corrected the vertical component for its inferred κ value. We observe that the effect of attenuation is negligible until 8–10 Hz. This is true not only for the traces shown in Fig. 2 but for all the records we studied. Attenuation measured in the IPOC stations in northern Chile is weak because these stations were installed in rock and there are no large, shallow sedimentary basins except in the Mejillones peninsula.

Once the acceleration spectra were corrected for anelastic attenuation, we computed the displacement spectra and we inverted M_0 and f_c assuming that the far-field spectra obey Brune's ω^{-2} model,

$$\Omega(f) = \frac{\Omega_0}{[1 + (f/f_c)^4]^{1/2}}, \quad (2)$$

where Ω_0 is the low-frequency spectral amplitude, f is the frequency, f_c is the corner frequency. $\Omega(f)$ is the displacement spectrum given by the vector composition of the spectra evaluated for the three components. Following Abercrombie (1995), the spectra were inverted for f_c using the Nelder–Meade simplex algorithm in the (0.01–10) Hz frequency range. We invert separately the spectrum at each station. For each event, the M_0 and the f_c were computed averaging over the available strong motion stations, and the uncertainty was computed from the standard deviation.

3.2 Estimation of radiated seismic energy

The computation of E_r requires an integration of the E_r flux across every station. This measurement is not trivial, because it is very sensitive to anelastic attenuation, radiation pattern and finite bandwidth effects. We evaluate the E_r using a method similar to Boatwright *et al.* (2002),

$$E_r = 8\pi r^2 C^2 \rho(x) \beta(x) \int_0^\infty \exp(2\pi k f) |\dot{u}(x, f)|^2 df, \quad (3)$$

where $\dot{u}(x, f)$ is the Fourier transform of ground velocity, r is the distance from source to observer, $\rho(x)\beta(x)$ is the seismic impedance and C contains the free-surface amplification and the radiation pattern. The effect of attenuation was corrected by the exponential decay already described in (1).

We must correct E_r also for the effect of the finite spectral bandwidth of observations using the ratio between the estimated and the

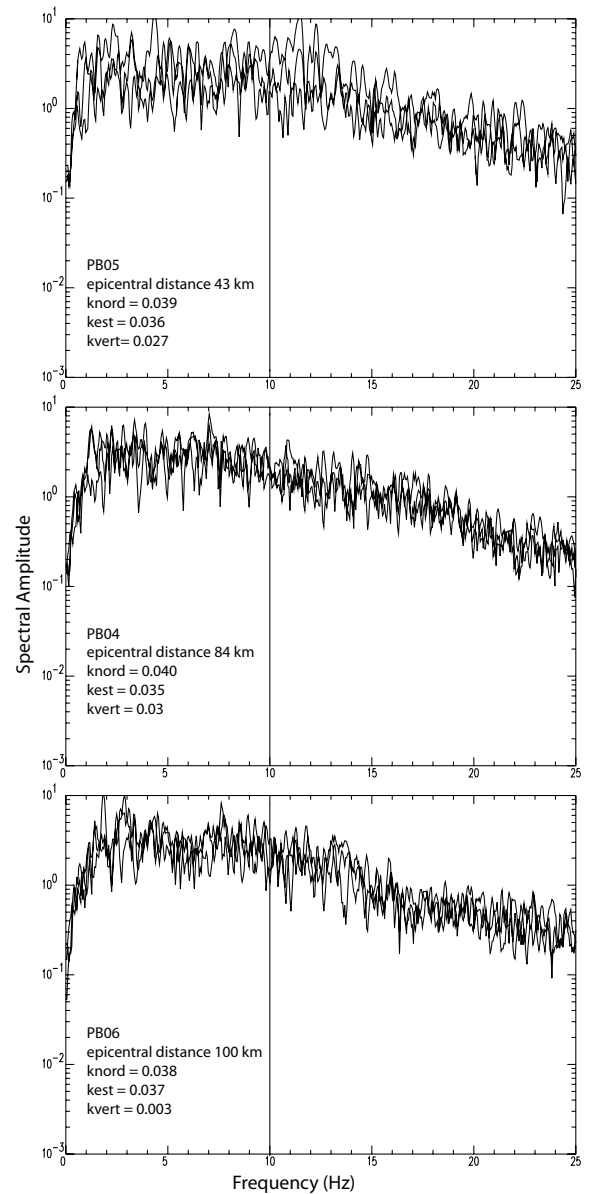


Figure 2. Acceleration spectra in linear-logarithm scale for the M_w 6.3 aftershock of 2007 November 15 plotted at the three closest stations. The black line at 10 Hz indicates the maximum frequency for the spectral inversion. For each station, we report the epicentral distance and the κ value of the attenuation correction.

true energy flow R (Di Bona & Rovelli 1988; Ide & Beroza 2001).

$$R(f_M, f_c) = \frac{2}{\pi} \frac{-f_M/f_c}{1 + (f_M/f_c)^2} + \arctan(f_M/f_c), \quad (4)$$

where f_M is the maximum observed frequency.

4 SPECTRAL BEHAVIOUR

Fig. 3 shows the scaling of the spectra of our 68 aftershocks in the graphical manner proposed initially by Aki (1967) and implemented by Prieto *et al.* (2004) for a set of small events in Southern California. Each spectrum is the average of the spectra evaluated at the stations located within 110 km from the epicentre. The dashed lines are ω^{-3} lines. In Fig. 3(b), we collapse all the spectra (corrected

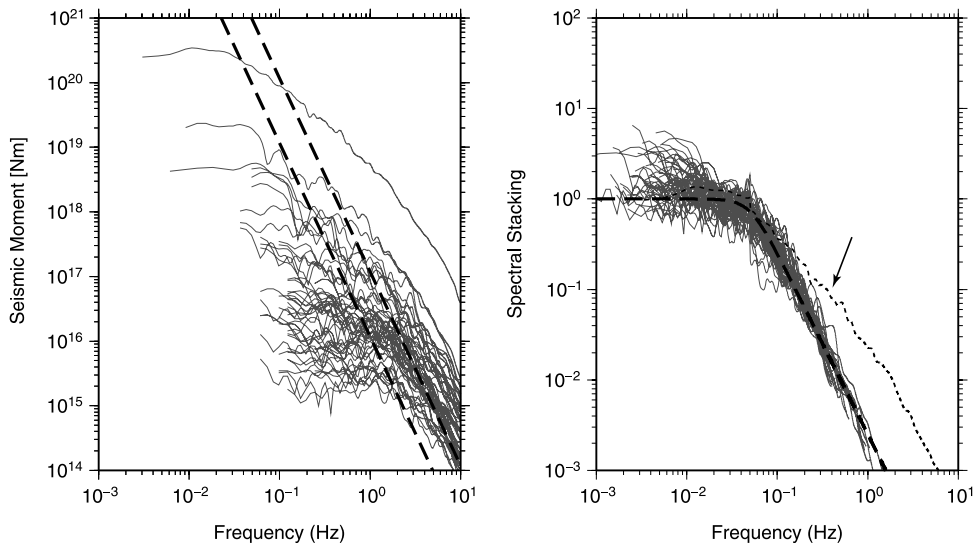


Figure 3. Graphical scaling of spectra. Left-hand panel: displacement spectra for all the studied events, each spectrum is the average of the spectrum observed over all available stations (epicentral distances <100 km). The dashed lines are ω^{-3} curves. Right-hand panel: spectral staking obtained shifting spectra along the ω^{-3} curve, and normalized to 1 by dividing each spectrum by seismic moment. The bold dash curve is an ω^{-2} spectrum, plotted as reference. The dashed line (indicated by the arrow) is the spectrum of the main event that is clearly different from that of the aftershocks due to near-field effects (see text for further discussion).

for κ) into a single figure, taking the ratio between the observed and theoretical spectra (Imanishi *et al.* 2004; Prieto *et al.* 2004). This figure clearly shows that the main event does not follow an omega-square spectral model. The reason is that the strong motion instruments are located at less than 110 km from the hypocentre so that near-field terms are important. All the other aftershocks follow the ω^{-2} model; the continuous slope indicating that the anelastic attenuation has been correctly removed from the spectra.

We carefully analysed the spectral behaviour of the main event spectral; the results are summarized in Fig. 4. On the left-hand panel,

we show the accelerograms recorded at the PB04, PB05, PB06 and PB07 stations (unfortunately the PB03 station did not record the main event), all these stations are located near the rupture area (see Fig. 1). We inverted the spectra (grey line in Fig. 4b) using both the ω^{-1} (dashed-point lines in the figure) and the ω^{-2} (dashed lines) models. The ω^{-1} model fits well the low-frequency signal, the inverted plateau value is 2.53×10^{20} Nm compatible with the moment magnitude of 7.7 of the Tocopilla earthquake. At higher frequencies ($f > 0.1$ Hz), the spectral decay is better described by the ω^{-2} model. The continuous black line, obtained by merging

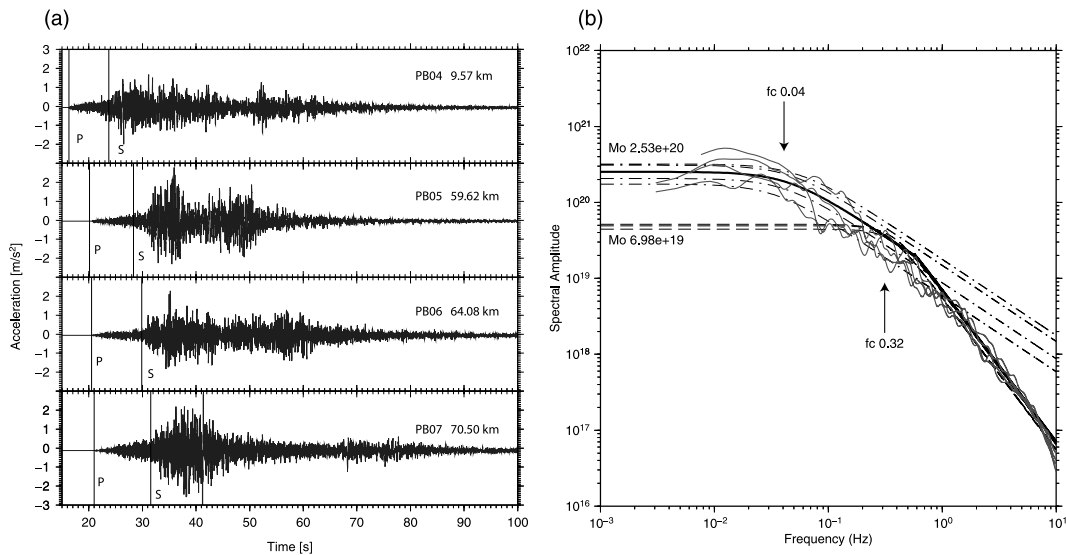


Figure 4. Spectra of the main Tocopilla event of 2007 November 14, $M_w = 7.7$. Left-hand panel (A), EW component of strong motion records of the main event at the four closest stations. On each record, we report the P and S arrivals and the epicentral distance, we used a window of 50 s around the S wave that includes the signals from the two slip patches shown in Fig. 1. Right-hand panel (B), the corresponding spectra. Grey lines are the displacement spectra at each station; each spectrum is the vector composition of the three components. Dashed-point lines, show the theoretical spectra inverted using a ω^{-1} model; dashed lines show the theoretical spectra inverted using an ω^{-2} model. The black solid line shows the spectrum obtained using the ω^{-1} model until 0.32 Hz and ω^{-2} at higher frequencies.

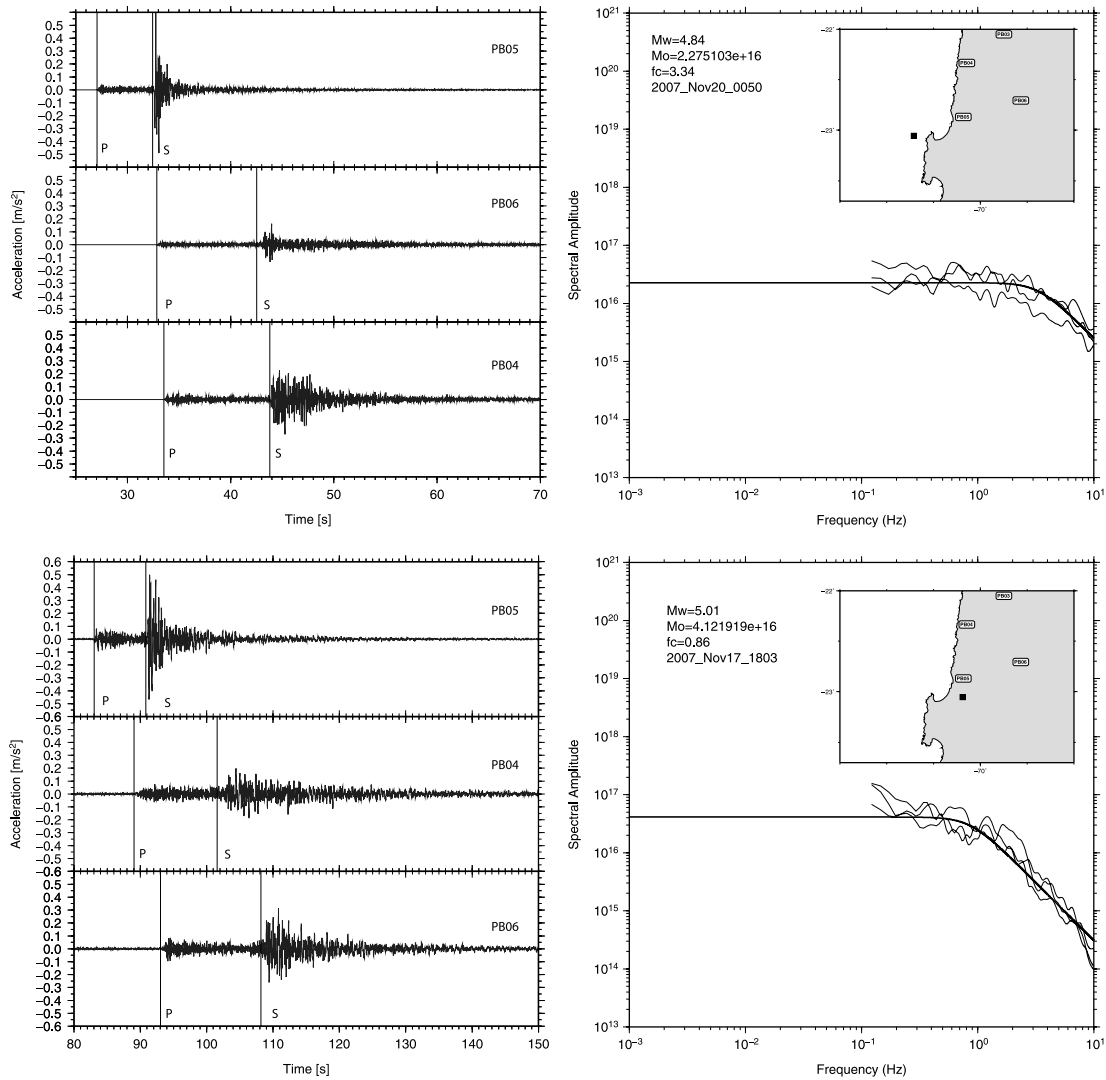


Figure 5. Comparison between waveforms and spectra for two events with the same magnitude but different f_c . For both events, we show the EW components at three closest stations. The spectra plotted on the right-hand panel are the average of the three spectra evaluated at the PB04, PB05 and PB06 stations.

the two spectral inversions, is the proposed seismic spectrum of the main event: at low frequencies the signal is dominated by the near-field radiation whose spectral decay is modelled using the ω^{-1} model, while the ω^{-2} fits well the spectral behaviour at high frequencies. Two corner frequencies characterize the spectrum at 0.04 and 0.32 Hz. The low-frequency scatter of spectra in Fig. 3(b) shows that not all the events have identical spectral properties. In Fig. 5, we compare the spectra of two aftershocks that occurred at two different moments of the sequence. One is located in-land the other is located offshore the Mejillones peninsula. On the left-hand panel, we plot the east–west component at PB05, PB04 and PB06 stations for both events. The events have similar moment magnitude, and the waveforms show some similarities (same S phase amplitude and duration at the recording stations). The spectral behaviour for these events is, however, quite different as shown in the plot on the right. Such an observation is important for the interpretation of the results presented in the following sections.

5 SCALING LAWS FOR THE TOCOPILLA SEQUENCE

We first investigated the scaling law of seismic spectrum without making any hypothesis about the fracture geometry (for instance, we did not use Brune’s circular fault model in this study). We looked for the relationships between the three parameters we retrieved from the spectra: the M_0 , the E_r and the f_c . In Fig. 6(a), we plot the f_c as a function of M_0 for the Tocopilla aftershocks seismic sequence. For each event f_c and M_0 are the average over all the stations, and are plotted along with the statistical errors. Individual measurements are plotted as small grey dots on the same figure. The scattering of the f_c reflects the different spectral properties discussed in previous section. For the main shock, we used the f_c inverted using an ω^{-1} model, this measure is reported only to give a complete overview on all the catalogue, because we have no way to correct for near-field effects. The dashed lines in Fig. 6 are lines of constant slope f_c^{-3} .

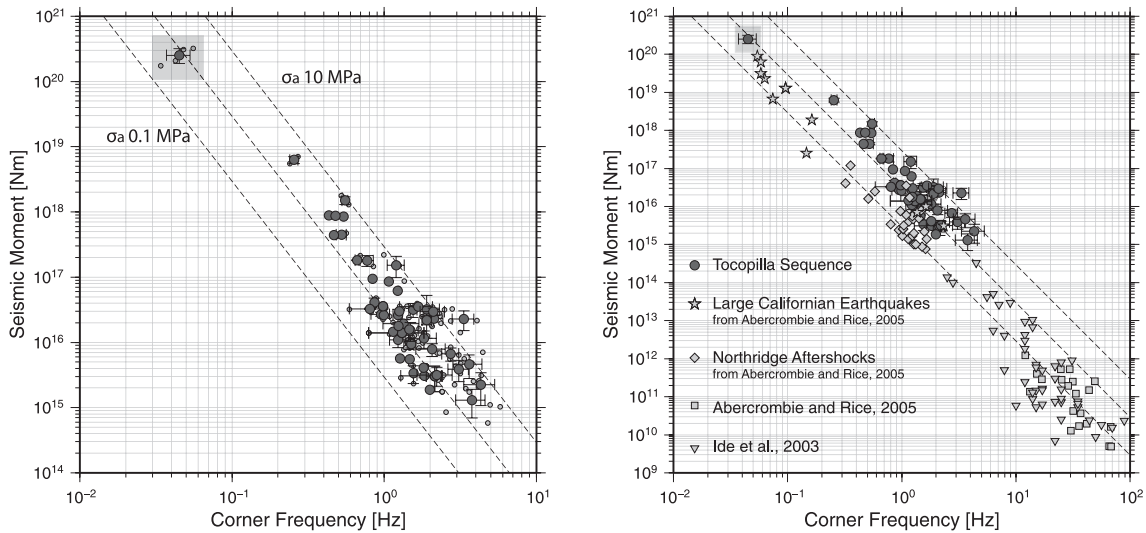


Figure 6. Corner frequency versus seismic moment. Left-hand panel: Results obtained for the Tocopilla aftershock sequence. Each point is the average of f_c and M_0 measured on all available stations for each event. They are plotted along with the statistical uncertainties. The small grey dots are the values estimated for each station. Right-hand panel: Comparison with the previously published results. In both figures, the dashed lines are the f_c^{-3} trend obtained using a constant σ_a ranging from 0.1 to 10 MPa; the lines have been estimated from eq. 6 assuming $C_r = 2$. For the sake of completeness, we plot the f_c estimated for the main shock, hidden by a grey panel.

On these lines the apparent stress, defined as,

$$\sigma_a = \mu \frac{E_r}{M_0}, \quad (5)$$

is constant varying from 0.1 and 10 MPa. In Fig 6(b), we compare the results obtained for the northern Chile earthquakes with the Californian events studied by Abercrombie (1995), Abercrombie & Rice (2005), Ide *et al.* (2003) and Mori *et al.* (2003). The Chilean events follow the same f_c^{-3} as events in California, but they have a higher value of apparent stress drop, between 1 and 10 MPa for northern Chile and between 0.1 and 1 MPa for California. This is not due to a higher value of μ that could at most explain a factor of 2.

In Fig. 7, we plot the apparent stress as a function of the M_0 (moment magnitude) along with their uncertainties. On the bottom-left-hand panel, we show the results obtained for the Tocopilla sequence. σ_a varies from 0.5 to 10 MPa. The σ_a estimates are characterized by a large scatter in the $10^{15} < M_0 < 10^{17}$ Nm range. We argue that this is related to the different spectral behaviour of the events, as discussed in the previous subsection. On the bottom-right-hand panel, we also show the effect of attenuation and finite bandwidth corrections; these corrections are very important for smaller events while they do not affect significantly the σ_a estimates for larger events. On the top panel of Fig. 7, we compare our estimates of σ_a together with those published by several authors. An alternative way to look at the σ_a scaling is presented in Fig. 8 where we plot E_r in function of M_0 , the dashed lines corresponds to constant σ_a values. As a general remark, the Tocopilla sequence shows a good agreement with data published by Mayeda & Walter (1996). In this figure, σ_a seems to scale with moment, we are, however, cautious in interpreting this result as violation of similarity, since the measurements are quite scattered and affected by large uncertainties.

5.1 The non-dimensional ratio, C_r

To obtain a more quantitative estimation of spectral scaling, it is convenient to introduce a non-dimensional parameter that quantifies

the fits of Fig. 3. For this purpose we use the ratio, C_r , defined in Appendix A,

$$C_r = \frac{\mu E_r \beta^3}{M_0^2 f_c^3}, \quad (6)$$

where β is the shear wave speed and μ the shear modulus. If M_0 scales with f_c as proposed by Aki (1967), $M_0 \propto f_c^{-3}$, and source dynamics is such that E_r/M_0 is scale independent, C_r should be constant for all earthquakes in the data set. The value of the constant depends on the details of the model; for the particular case of Brune's spectral model, C_r should be approximately equal to 2 (see Appendix A).

In Fig. 9, we plot the non-dimensional ratio, C_r , as a function of M_0 . For the Tocopilla aftershocks, C_r is distributed around 2.0 with the exception of the main event that, as we have previously discussed, is affected by near-field effects. The C_r values computed using data from other authors are more scattered. This can be explained in terms of experimental errors or due to source complexity not present in our data set.

As a partial conclusion, the Tocopilla aftershocks seem to satisfy the scaling law as measured by the C_r ratio in spite of the obvious differences in signal shape shown in Fig. 5. We tested this hypothesis without any reference to a particular source model. The only assumption used so far is that earthquake spectra are of the ω^{-2} shape, defined by eq. (2).

6 THE SCALING OF ENERGY RELEASE RATE WITH EARTHQUAKE SIZE

In this section, we will investigate the scaling relationship between the energy release rate and the size of the rupture. For this purpose, we need to introduce a specific geometry of the fracture model. We use the static circular model because it has an extremely simple formulation and has been used by previous authors (Abercrombie & Rice 2005).

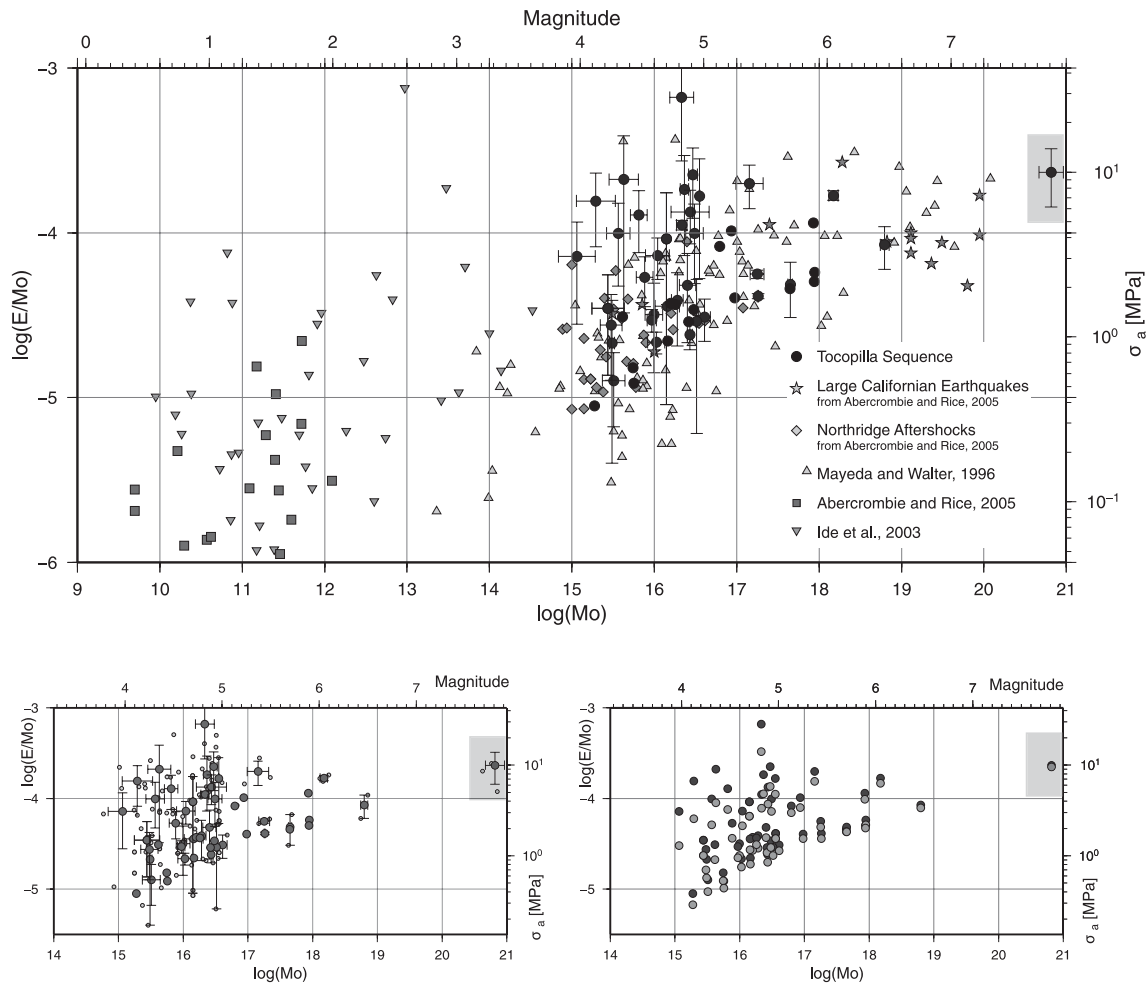


Figure 7. Ratio of radiated energy to seismic moment as a function of seismic moment. Top panel: Comparison with the results published by other authors. The plotted value of E_r/M_0 is the average over all the stations per event, plotted along with the uncertainties. The statistical error is the propagation of the errors on E_r and M_0 . Bottom left-hand panel: E_r/M_0 as a function of M_0 for the Tocopilla events. The small grey dots are the value computed at each station. Bottom right-hand panel: Effect of the attenuation and finite bandwidth corrections. In grey, the uncorrected estimate, in black, the corrected values.

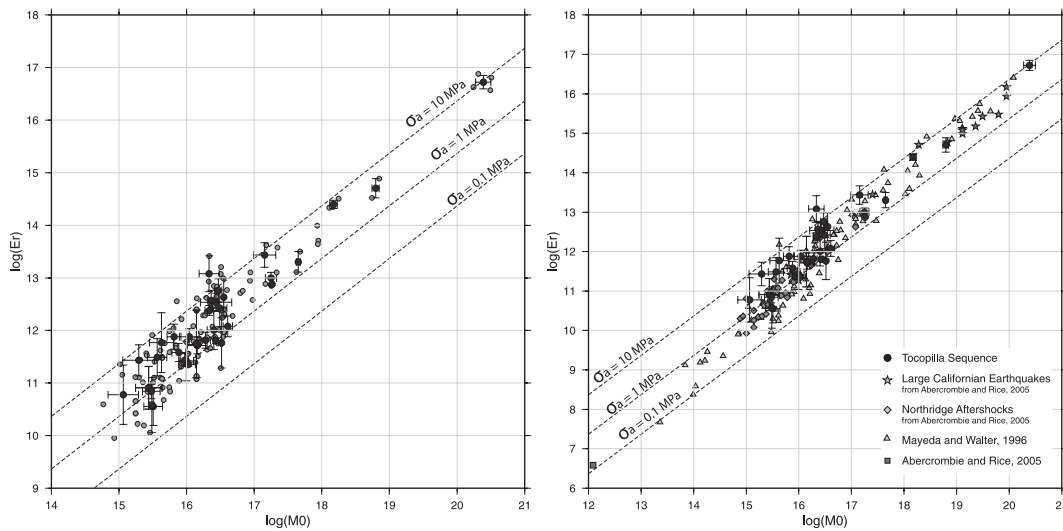


Figure 8. Radiated energy as a function of seismic moment. Left-hand panel: E_r as a function of M_0 for Tocopilla events. The small grey dots are the value computed at each station. Right-hand panel: Comparison with the results published by other authors (see legend) with finite bandwidth corrections. In grey, the uncorrected estimate, in black, the corrected values.

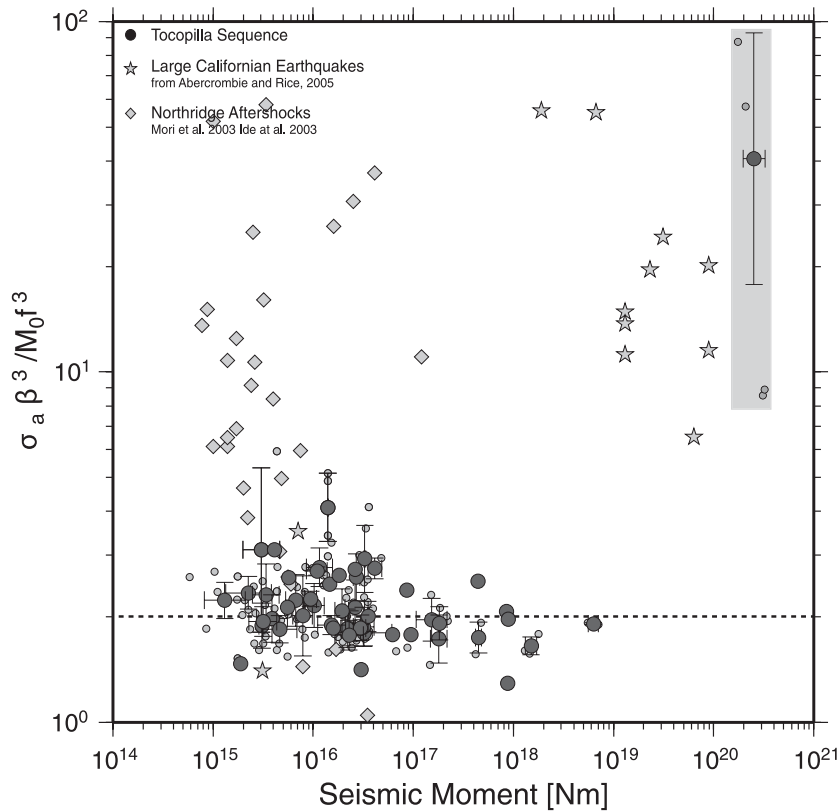


Figure 9. The non-dimensional ratio C_r versus seismic moment. The circles represent the C_r values computed for the Tocopilla aftershock sequence. The values of C_r are averaged over the available stations for each event. They are plotted along with their uncertainties. The statistical errors is the propagation of the errors. We also plot with different symbols C_r estimated from published data. We report inside a grey box the results for the main event.

6.1 Energy flow rate

An earthquake is a propagating shear crack controlled by available strain energy that is released by faulting. This available energy is used, in part, to emit seismic waves and, in part, to make the fracture propagate. The energy balance for this process was established by Kostrov (1974), and has been reviewed by numerous authors, including Rivera & Kanamori (2005). Using the notation of eq. (24) of the latter authors, we write the energy balance as,

$$E_r = \Delta W - E_G - E_F, \quad (7)$$

where E_r is the total radiated energy as observed in the far field, E_G is the fracture energy used to propagate the rupture and E_F is the so-called Kostrov term, the energy dissipated due to fast changes of stress on the fault. The available strain energy is,

$$\Delta W = \int_S \Delta\sigma D dS, \quad (8)$$

where D is the slip and $\Delta\sigma$ is the static stress drop, defined as the difference between the initial and the final stress on the fault plane.

$$\Delta\sigma = T_0 - T_f. \quad (9)$$

It is important to note that ΔW is not the total strain energy change during the earthquake, it is only that part of the energy change that is available to be radiated. To compute the total energy change, we would need to know the energy dissipated by friction, but this could only be computed if we knew the absolute stress level, something that can not be computed from seismic data alone (Madariaga 2010).

In the following, we assume that the Kostrov term is either neglected or incorporated into the fracture energy term. We write then in general,

$$E_G = \int_S G_c dS, \quad (10)$$

where G_c is the energy release rate: the amount of energy required to make the crack surface advance per unit surface. In our view, the energy release rate includes not only the actual surface energy but also energy dissipated by damage, melting and other fast processes that occur on the fault. Different assumptions about the variation of G_c with size of the fault will be made in the following.

To compute ΔW using eq. (8), we have to assume a specific fracture model describing the distribution of stress on the fault plane and the geometry of the fault. For simplicity and because we do not know the exact shape of the aftershocks, we assume a planar static circular crack of radius a with a constant static stress drop $\Delta\sigma$. The slip distribution, D , on a circular fault is (Eshelby 1957; Keilis-Borok 1959),

$$D(r) = \frac{24}{7\pi} \frac{\Delta\sigma}{\mu} \sqrt{a^2 - r^2}, \quad (11)$$

where r is the radial distance from the centre of the crack, a is the radius of the crack and the static stress drop, $\Delta\sigma$, is related to the scalar moment, M_0 through the equation,

$$M_0 = \frac{16}{7} \Delta\sigma a^3. \quad (12)$$

Substituting eq. (11) into eq. (8), and integrating over the fault area, we obtain the static energy change (Ide 2002),

$$\Delta W = \frac{8}{7} \frac{\Delta\sigma^2}{\mu} a^3. \quad (13)$$

We have to estimate the E_r for the circular shear crack. This was estimated by Madariaga (1976) for different speeds. Here, we will assume, as Brune (1970) did, that the f_c is given by,

$$f_c = \frac{0.372\beta}{a}, \quad (14)$$

where a is the equivalent radius of the fault. As shown by Brune, the numerical value 0.372 implies that the E_r is a well-defined fraction of the available energy. For Brune's model, we prove in Appendix B that the E_r is ~ 46 per cent of the strain energy release so that,

$$E_r = 0.466\Delta W, \quad (15)$$

so that the energy release rate can be approximated by,

$$G_c S \approx \frac{1}{2} \Delta W. \quad (16)$$

Assuming now that for a particular earthquake G_c is independent of position on the fault, we get the average expression,

$$G_c \approx \frac{1}{2} \frac{\Delta W}{\pi a^2} = \frac{4}{7\pi} \frac{\Delta\sigma^2}{\mu} a, \quad (17)$$

where a the source radius that we compute from f_c using,

$$a = \frac{0.372\beta}{f_c}, \quad (18)$$

and $\Delta\sigma$ is computed from the moment and fault radius by,

$$\Delta\sigma = \frac{7}{16} \frac{M_0}{a^3}. \quad (19)$$

In the computation of G_c , we used the shear wave velocity, β , from the model by Husen *et al.* (1999), and f_c and M_0 were determined from the displacement spectra (eq. 2). Expression (17) was computed independently for every event in our catalogue.

A somewhat different approximation was used by Abercrombie & Rice (2005) who proposed that G_c is given by,

$$G_c = \frac{1}{2} (\Delta\sigma - 2\sigma_a) D, \quad (20)$$

where $\Delta\sigma$ is the static stress drop and σ_a is the apparent stress defined in eq. (2), and the average slip, D , is determined from the M_0 .

The two formulations are equivalent but make different assumptions about the ratio between radiated and strain energy. Both expressions (17) and (20) will be tested on the *Tocopilla* data set.

6.2 Scaling of G_c for the *Tocopilla* events

In Fig. 10, we plot G_c as a function of M_0 (top panel) and as a function of slip (bottom panel) together with the results published by Abercrombie & Rice (2005) (many of the G_c values were computed by Abercrombie and Rice using the source parameters estimated by Ide *et al.* (2003); Mori *et al.* (2003) and other authors cited in table 5 of their paper). On the left-hand side of Fig. 10, we plot the G_c values derived using eq. (17), and on the right-hand side, those retrieved using the expression (20). We observe that G_c scales with slip and its values range between 10^4 and 10^7 Jm⁻², in agreement with results published by other authors. Also, the plots on the left-

and right-hand side are similar, confirming the equivalence of the two formulations presented so far. The trend observable on Chilean data is in agreement with that of Northridge aftershocks (the grey diamonds), but those data do not follow the same trend of the small events.

To better understand if G_c scales with event size, we plot it as a function of the M_0 . Events with M_0 10^{14} – 10^{17} show scattered G_c values; indeed the dispersion shown by Chilean data is comparable with that of the Californian events. Looking at the full M_0 range, it appears that data follows a linear trend. However, we do not show any linear regression since it is not statistically significant; this is due to the large scatter displayed by the smaller events and to the lack of observations for $M_0 > 10^{17}$.

7 CONCLUSIONS

We found from graphical methods (Fig. 3b) and analytical methods (Fig. 10) that the spectra of the aftershocks of the *Tocopilla* earthquake of 2007 November 14 are self-similar. This conclusion is supported by the investigation of three scaling relationships: the Aki scaling law of the seismic spectrum, the invariance of the apparent stress drop with the earthquake size and the invariance of the non-dimensional constant C_r with the event size.

The C_r parameter, introduced by Madariaga (2010) and defined in Appendix A, is investigated for the first time on an original data set in this paper. It is a non-dimensional constant proportional to the ratio between the apparent stress drop and the product of the moment and the cube of the f_c : two quantities supposed to be scale independent. Since three parameters are used to describe the source (moment, f_c and E_r ; the parameters are related to the source dimension and stress drop), to properly demonstrate the earthquakes invariance it is necessary to investigate three scaling relationships. Usually authors (Abercrombie 1995; Abercrombie & Rice 2005; Oth *et al.* 2010) introduce as a third scaling relationship, the scaling of static stress drop. But this depends on the particular dynamic fracture model used to compute stress drop. The advantage of the C_r parameter is that does not rely on any specific model of the source. The particular value of C_r that fits the data may be used to discriminate between different fault models. For earthquake whose spectra are well-modelled by omega-squared type (2), C_r should be close to 2 (see eq. A11). This number is independent of any geometry and assumption about stress drop. It is just based on the omega-squared model. This is the case with the data set that we examined here. We conclude that the aftershocks of the *Tocopilla* earthquake are scale independent within a ratio of 2 of the average value of C_r .

We also studied the scaling of the energy release rate (or fracture energy) G_c with event size. The motivation behind this specific study comes from our recent observation (Lancieri *et al.* 2011) that the the integral of the squared velocity measured during a few seconds of P and S phases scales with the event size. A possible explanation of those relationships was proposed by Nielsen (2006) in terms of the scaling of G_c with the event size. The scale dependence of G_c is still a matter of debate because it is difficult to estimate from seismograms (Beroza & Spudich 1988; Ide 2003; Tinti *et al.* 2005). In this paper, we measured G_c directly from the spectral parameters following and approach similar to that of Abercrombie & Rice (2005). We also made two additional assumptions: we adopted the static circular crack as rupture model and the Brune model for the energy partition (see Appendix B). We get a simpler expression for G_c than that of Abercrombie & Rice (2005) that we also used to

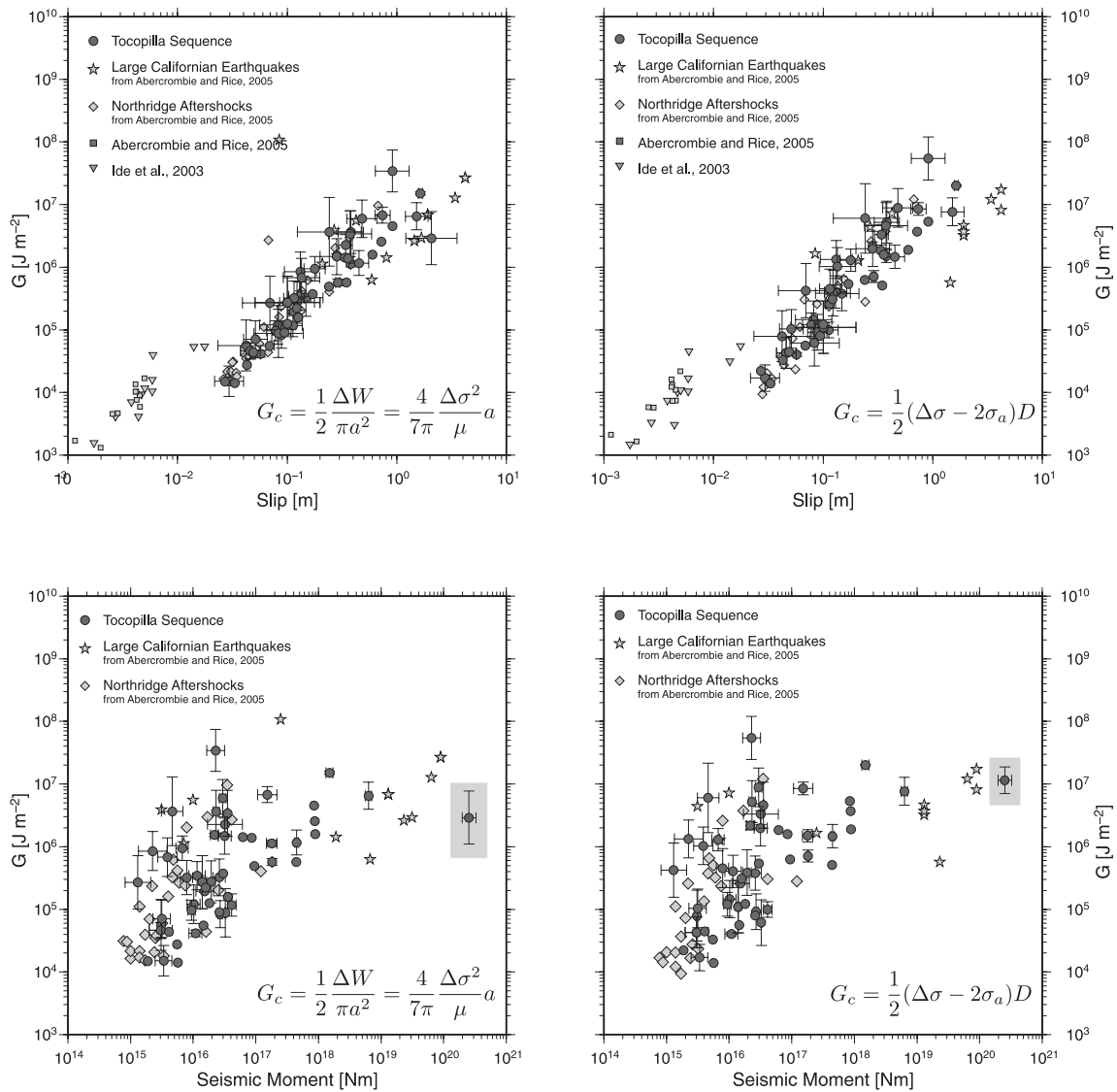


Figure 10. Energy release rate G_c as a function of moment and slip. Left-hand column: Energy release rate obtained using Brune's spectral model (shown as inset as bottom right-hand panel). Right-hand column: Energy release rate computed assuming the Abercrombie & Rice (2005) formulation shown also in the inset. Top row: G_c as a function of slip, we omitted the main event, bottom row: G_c as a function of seismic moment. We report in the grey box the results for the main event.

estimate energy release rate. Both approaches yield values of G_c that are similar and that clearly scale with the size of the event, although there is a large scatter.

ACKNOWLEDGMENTS

This research was carried out under FONDECYT contract 1100429 in Chile and of contract ANR DEBATE in France. This research was carried out under the Montessus de Ballore International Laboratory established between the University of Chile and the Centre National de la Recherche Scientifique (CNRS) in France. Many researchers made possible this research, most notably A. Nercessian, S. Barrientos, M. Sobieziak, G. Meneses. We thank B. Schurr and other colleagues at GFZ who deployed the plate boundary stations in northern Chile. A special thank to A. Fuenzalida for her work on refining the aftershocks location, and to S. Ruiz, C. Satriano and O. Scotti for fruitful discussions. We also thank the editor F. Krueger, P.M. Mai and one anonymous reviewer for their comments that helped to improve the manuscript.

REFERENCES

- Abercrombie, R.E., 1995. Earthquake source scaling relationships from -1 to $5 M_l$ using seismograms recorded at 2.5-km depth, *J. geophys. Res.*, **100**(B12), 24 015–24 036, doi:10.1029/95JB02396.
- Abercrombie, R.E. & Rice, J.R., 2005. Can observations of earthquake scaling constrain slip weakening?, *Geophys. J. Int.*, **162**(2), 406–424, doi:10.1111/j.1365-246X.2005.02579.x.
- Aki, K., 1967. Scaling law of seismic spectrum, *J. geophys. Res.*, **72**(4), 1217–1231, doi:10.1029/JZ072i004p01217.
- Aki, K., 1979. Characterization of barriers on an earthquake fault, *J. geophys. Res.*, **84**, 6140–6148.
- Anderson, J.G. & Hough, S., 1984. A model for the shape of the Fourier amplitude spectrum of acceleration at high frequencies, *Bull. seism. Soc. Am.*, **74**(5), 1969–1993.
- Beroza, G. & Spudich, P., 1988. Linearized inversion for fault rupture behavior: application to the 1984 Morgan Hill, California, earthquake, *J. geophys. Res.*, **93**(B6), 6275–6296, doi:10.1029/JB093iB06p06275.

- Boatwright, J., 1980. A spectral theory for circular seismic sources: simple estimates of source dimension, dynamic stress drop, and radiated energy. *Bull. seism. Soc. Am.*, **70**, 1–26.
- Boatwright, J., Choy, G. & Seekins, L., 2002. Regional estimates of radiated seismic energy. *Bull. seism. Soc. Am.*, **92**, 1241–1255.
- Bonilla, L.F., Steidl, J.H., Lindley, G.T., Tumarkin, A.G. & Archuleta, R.J., 1997. Site amplification in the San Fernando Valley, California: variability of site-effect estimation using the S-wave, Coda, and H/V methods. *Bull. seism. Soc. Am.*, **87**(3), 710–730.
- Brune, J., 1970. Tectonic stress and the spectra of seismic shear waves from earthquakes. *J. geophys. Res.*, **75**(26), 4997–5009, doi:10.1029/JB075i026p04997.
- Chlieh, M., de Chabaliere, J.B., Ruegg, J., Armijo, R., Dmowska, R., Campos, J. & Feigl, K.L., 2004. Crustal deformation and fault slip during the seismic cycle in the North Chile subduction zone, from GPS and InSAR observations. *Geophys. J. Int.*, **158**, 695–711, doi:10.1111/j.1365-246X.2004.02326.x.
- Choy, G. & Boatwright, J., 1995. Global patterns of radiated seismic energy and apparent stress. *J. geophys. Res.*, **100**(B9), doi:10.1029/85JB01969.
- Das, S., 1976. A numerical study of rupture propagation and earthquake source mechanisms. *PhD thesis*, Massachusetts Institute of Technology, Cambridge, MA.
- Delouis, B., Pardo, M., Legrand, D. & Monfret, T., 2009. The M_w 7.7 Tocopilla earthquake of 14 November 2007 at the southern edge of the Northern Chile seismic gap: rupture in the deep part of the coupled plate interface. *Bull. seism. Soc. Am.*, **99**(1), 87–89, doi:10.1785/0120080192.
- Di Bona, M. & Rovelli, A., 1988. Effects of the bandwidth limitation of stress drops estimated from integrals of the ground motion. *Bull. seism. Soc. Am.*, **78**(5), 1818–1825.
- Eshelby, J., 1957. The elastic field of an ellipsoid inclusion and related problems. *Proc. R. Soc.*, **241**(1226), 376–396.
- Guatteri, M., Spudich, P. & Beroza, G., 2001. Inferring rate and state friction parameters from a rupture model of the 1995 Hyogo-ken Nanbu (Kobe) Japan earthquake. *J. geophys. Res.*, **106**(B6), 26 511–26 521.
- Husen, S., Kissling, E., Flueh, E. & Asch, G., 1999. Accurate hypocentre determination in the seismogenic zone of the subducting Nazca Plate in northern Chile using a combined on-/offshore network. *Geophys. J. Int.*, **138**, 3687–3701, doi:10.1046/j.1365-246x.1999.00893.x.
- Hussein, M.I., Jovanovich, D.B., Randall, M.J. & Freund, L.B., 1975. The fracture energy of earthquakes. *Geophys. J. R. astr. Soc.*, **43**, 367–385.
- Ide, S., 2002. Estimation of radiated energy of finite-source earthquake models. *Bull. seism. Soc. Am.*, **92**, 2994–3005, doi:10.1785/0120020028.
- Ide, S., 2003. Fracture surface energy of natural earthquake from the viewpoint of seismic observation. *Bull. Earth. Res. Inst.*, **78**, 59–65.
- Ide, S. & Beroza, G.C., 2001. Does apparent stress vary with earthquake size?. *Geophys. Res. Lett.*, **28**(17), 3349–3352, doi:10.1029/2001GL0131106.
- Ide, S., Beroza, G., Prejean, S. & Ellsworth, W., 2003. Apparent break in earthquake scaling due to path and site effects on deep borehole recordings. *J. geophys. Res.*, **108**(B5), doi:10.1029/2001JB001617.
- Imanishi, K., Ellsworth, W. & Prejean, S., 2004. Earthquake source parameters determined by the safod pilot hole seismic array. *Geophys. Res. Lett.*, **31**, L12S09, doi:10.1029/2004GL019420.
- Izutani, Y. & Kanamori, H., 2001. Scale-dependence of seismic energy-to-moment ratio for strike-slip earthquakes in Japan. *Geophys. Res. Lett.*, **28**(20), 4007–4010, doi:10.1029/2001GL013402.
- Kanamori, H., 1977. The energy release in great earthquakes. *J. geophys. Res.*, **82**, 2921–2987, doi:10.1029/JB082i020p02981.
- Kanamori, H., Mori, J., Hauksson, E., Heaton, T., Hutton, L. & Jones, L., 1993. Determination of earthquake energy release and MI using terracope. *Bull. seism. Soc. Am.*, **83**(2), 330–346.
- Keilis-Borok, V., 1959. On estimation of the displacement in an earthquake source and of source dimensions. *Ann. Geofis. (Rome)*, **12**, 205–214.
- Kostrov, B.V., 1964. Selfsimilar problems of propagation of shear cracks. *Appl. Math. Mech.*, **28**(5), 1077–1087.
- Kostrov, B.V., 1974. Seismic moment and energy of earthquakes, and seismic flow of rocks. *Izv. Earth Phys.*, **1**, 23–40.
- Lancieri, M., Fuenzalida, A., Ruiz, S. & Madariaga, R., 2011. Magnitude scaling of early-warning parameters for the M_w 7.8, Chile, earthquake and its aftershocks. *Bull. seism. Soc. Am.*, **101**(2), doi:10.1785/0120100045.
- Madariaga, R., 1976. Dynamics of an expanding circular fault. *Bull. seism. Soc. Am.*, **66**(3), 639–666.
- Madariaga, R., 2010. Earthquake scaling laws, in *Extreme Environmental Events: Complexity in Forecasting and Early Warning*, ed. Meyers, R. Springer, Berlin, doi:10.1007/978-1-4419-7695-6, ISBN: 978-4419-7694-9.
- Matsuzawa, T., Takeo, M., Ide, S., Iio, Y., Ito, H., Imanishi, K. & Horiuchi, S., 2004. S-wave energy estimation of small-earthquakes in the Western Nagano Region, Japan. *Geophys. Res. Lett.*, **31**(3), L03 602, doi:10.1029/2003GL018445.
- Mai, P.M., Somerville, P., Pitarka, A., Dalguer, L., Miyake, H., Beroza, G., Song S.-G. & Irikura, K., 2006. Fracture-energy scaling in dynamic rupture models of past earthquakes, in *Earthquakes: Radiated Energy and the Physics of Faulting*, Geophys. Monogr. Ser. 170, pp. 283–294, eds McGarr, A., Abercrombie, R., Kanamori, H., American Geophysical Union, Washington, DC.
- Mayeda, K. & Walter, W., 1996. Moment, energy, stress drop, and source spectra of western united states earthquakes from regional coda envelopes. *J. geophys. Res.*, **101**(B5), doi:10.1029/96JB00112.
- Mayeda, K., Malagnini, L. & Walter, W., 2007. A new spectral ratio method using narrow band coda envelopes: evidence for non-self-similarity in the Hector mine sequence. *Geophys. Res. Lett.*, **34**(11), L11303, doi:10.1029/2007GL030041.
- McGarr, A., 1999. On relating apparent stress to the stress causing earthquake fault slip. *J. geophys. Res.*, **104**(B2), 3003–3011, doi:10.1029/1998JB900083.
- Mori, J., Abercrombie, R. & Kanamori, H., 2003. Stress drop and radiated energies of aftershocks of the 1994 Northridge, California, earthquake. *J. geophys. Res.*, **108**, doi:10.1029/2001JB000474.
- Nielsen, S., 2006. Can earthquake size be controlled by the initial seconds of rupture?, in *Earthquake Early Warning Systems*, ed. Gasparini, P., Manfredi, G. & Zhao, J., Springer, Berlin, ISBN:978-3-540-72240-3.
- Ohnaka, M., 2003. A constitutive scaling law and a unified comprehension for frictional slip failure, shear fracture of intact rock, and earthquake rupture. *J. geophys. Res.*, **108**, doi:10.1029/2000JB000123.
- Oth A., Bindi, D., Parolai, S. & Di Giacomo, D., 2010. Earthquake scaling characteristics and scale-(in)dependence of seismic energy-to-moment ratio: insights from KiK-net data in Japan. *Geophys. Res. Lett.*, **37**, doi:10.1029/2010GL044572.
- Perez-Campos, X. & Beroza, G.C., 2001. An apparent mechanism dependence of radiated seismic energy. *J. geophys. Res.*, **106**(B6), doi:10.1029/2000JB9000455.
- Peyrat, S., Madariaga, R., Buforn, E., Campos, J., Asch, G. & Vilotte, J., 2010. Kinematic rupture process of the 2007 Tocopilla earthquake and its main aftershocks from teleseismic and strong motion data. *Geophys. J. Int.*, **182**(3), 1411–1430, doi:10.1111/j.1365-246X.2010.04685.x.
- Prejean, S. & Ellsworth, W., 2001. Observations of earthquake source parameters at 2 km depth in the Long Valley Caldera, Eastern California. *Bull. seism. Soc. Am.*, **91**(2), 165, doi:10.1785/0120000079.
- Prieto, G., Shearer, P., Vernon, F. & Kilb, D., 2004. Earthquake source scaling and self-similarity estimation from stacking P and S spectra. *J. geophys. Res.*, **109**, B08310, doi:10.1029/2004JB003084.
- Richardson, E. & Jordan, T., 2002. Low-frequency properties of intermediate-focus earthquakes. *Bull. seism. Soc. Am.*, **92**(6), 2434, doi:10.1785/0120010193.
- Rivera, L. & Kanamori, H., 2005. Representations of the radiated energy in earthquakes. *Geophys. J. Int.*, **162**, 148–155, doi:10.1111/j.1365-246X.2005.02648.x.
- Ruegg, J. et al., 1996. The $M_w = 8.1$ Antofagasta (North Chile) earthquake of July 30, 1995: first results from teleseismic and geodetic data. *Geophys. Res. Lett.*, **23**(9), 917–920, doi:10.1029/96GL01026.
- Sato, T. & Hirasawa, T., 1973. Body wave spectra from propagating shear cracks. *J. Phys. Earth*, **21**, 415–431.
- Scholz, C., 2002. *The Mechanics of Earthquakes and Faulting*, Cambridge University Press, Cambridge, ISBN 0-521-65540-4.

- Schurr, B. *et al.*, 2009. The International Plate Boundary Observatory Chile (IPOC) in northern Chile seismic gap, *Geophys. Res. Abstr.*, **11**, 11040.
- Stork, A. & Ito, H., 2004. Source parameter scaling for small earthquakes observed at the western Nagano 800-m-deep borehole, Central Japan, *Bull. seism. Soc. Am.*, **94**(5), 1781, doi:10.1785/012002214.
- Shearer, P.M., Prieto, G.A. & Hauksson, E., 2006. Comprehensive analysis of earthquake source spectra in southern California, *J. geophys. Res.*, **111**, doi:10.1029/2005JB003979.
- Singh, S. & Ordaz, M., 1994. Seismic energy release in Mexican subduction zone earthquakes, *Bull. seism. Soc. Am.*, **84**(5), 1533.
- Tinti, E., Spudich, P. & Cocco, M., 2005. Earthquake fracture energy inferred from kinematic rupture models on extended faults, *J. geophys. Res.*, **110**, doi:10.1029/2005JB003644.
- Yamada, T., Mori, J., Ide, S., Kawakata, H. & Iio, Y., 2005. Radiation efficiency and apparent stress of small earthquakes in a South African gold mine, *J. geophys. Res.*, **110**, B01305, doi:10.1029/2004JB003221.

APPENDIX A: THE NON-DIMENSIONAL RATIO, C_r

In this appendix, we derive the expression of the non-dimensional ratio, C_r , in eq. (6) proposed by Madariaga (2010). The three parameters that we measure from the spectra of aftershocks are the seismic moment, M_0 , the corner frequency, f_c and the radiated energy, E_r . Assuming that energy flow is dominated by S waves, we find from straightforward dimensional analysis of the equations of motion the following non-dimensional parameter,

$$C_r = \frac{\mu E_r^S \beta^3}{M_0^2 f_c^3}, \quad (\text{A1})$$

we added μ and β^3 to obtain the right dimensions. The non-dimensional ratio, C_r , may be considered as the quotient of σ_a defined by eq. (5) by a quantity $M_0/\mu \times \beta^3/f_c^3$, which is proportional to stress drop independently of any particular fault geometry.

We can derive the ratio, C_r , in another way using an expression of radiated energy derived by many authors (Boatwright 1980; Ide 2002). The far-field displacement, u_c , radiated by a point double couple source can be written in the following form:

$$u_c(r, t) = \frac{1}{4\pi\rho c^3} \frac{\mathcal{R}_c}{R} \Omega\left(t - \frac{R}{c}\right), \quad (\text{A2})$$

where c stands for P or S waves; ρ is the density; \mathcal{R}_c is the radiation pattern; R is the distance of the observation point to the source; $\Omega(t) = M_0 ds(t)/dt$ is the source time function; M_0 scalar moment and $s(t)$ is the time variation of the moment such that $\int s(t)dt = 1$.

Assuming that the source is embedded in a homogeneous medium, and the observation point is far from the source, the energy flow per unit solid angle, e_r is proportional to the square of the particle velocity v_c , so that the total flow per unit solid angle is,

$$e_r^c = \rho c R^2 \int_0^\infty v_c^2(t)dt, \quad (\text{A3})$$

where ρc is the seismic impedance. By substituting, v_c , with the derivative of the far-field displacement, \dot{u}_c ,

$$e_r^c = \frac{1}{16\pi^2 c^5} \mathcal{R}_c^2 \int_0^\infty \dot{\Omega}^2(t)^2 dt. \quad (\text{A4})$$

Applying the Parseval's theorem,

$$\int_0^\infty \dot{\Omega}^2(t)dt = \frac{1}{\pi} \int_0^\infty \omega^2 |\Omega(\omega)|^2 d\omega, \quad (\text{A5})$$

we compute the total E_r . Integrating over the angle θ and ϕ we get,

$$E_r^c = \frac{1}{4\pi^2 \rho c^5} \langle \mathcal{R}_c^2 \rangle \int_0^\infty \omega^2 |\Omega(\omega)|^2 d\omega, \quad (\text{A6})$$

where

$$\langle \mathcal{R}_c^2 \rangle = \frac{1}{4\pi} \int \int_\Omega \mathcal{R}_c^2(\theta, \phi) \sin\theta d\theta d\phi, \quad (\text{A7})$$

is the mean-squared radiation pattern. This formulation for the E_r does not depend on any assumption on earthquake dynamics, just on the shape of the spectrum. For the omega-square model (2), the integral over circular frequency is $\frac{\pi}{4} M_0^3 \omega_c^3$, so that the E_r is,

$$E_r^c = \frac{1}{16\pi} \langle \mathcal{R}_c \rangle^2 \frac{M_0^2 \omega_c^3}{\rho c^5} \quad (\text{A8})$$

Since E_r and moment have the same dimensional units, it is customary to rewrite the expression in the following non-dimensional form:

$$\frac{E_r^c}{M_0} = \frac{\pi^2 \langle \mathcal{R}_c \rangle^2}{2} \frac{M_0 f_c^3}{\rho c^5}, \quad (\text{A9})$$

where the circular f_c , ω_c , has been replaced by $2\pi f_c$.

For S waves, $c = \beta$ and $\mu = \rho\beta^2$ so that we can rewrite this expression as the non-dimensional number,

$$C_r = \frac{\mu E_r^S \beta^3}{M_0^2 f_c^3}. \quad (\text{A10})$$

In this expression, the ratio E_r/M_0 is non-dimensional, and so is $M_0/\mu \times \beta^3/f_c^3$, so that C_r is non-dimensional.

The average radiation pattern for the S phase $\langle \mathcal{R}_s \rangle^2 = 6/15$, so that for S waves,

$$C_r = 1.9739. \quad (\text{A11})$$

This non-dimensional relation makes no assumptions about the rupture process at the source except that the spectrum follows the model defined by eq. (2).

APPENDIX B: BRUNE MODEL FOR SEISMIC RADIATION

In the model proposed by Brune in 1970 for the S waves, the relation between the f_c and the fault size is,

$$f_c = 0.3724 \frac{\beta}{a}. \quad (\text{B1})$$

We can now derive a relationship between the radiated energy and the rupture energy. Assuming a planar static circular crack of radius, a , with constant stress drop $\Delta\sigma$ we can derive from (A1) the apparent stress drop,

$$\sigma_a = \mu \frac{E_r}{M_0} = C_r M_0 \frac{f_c^3}{\beta^3}, \quad (\text{B2})$$

where the non-dimensional constant, C_r , is assumed to be equal to 1.9739 as shown in (A11) of Appendix A. Using the definition of moment (12) and Brune's expression for the corner frequency we get the following relation between apparent and static stress drop:

$$\sigma_a = 0.2331 \Delta\sigma. \quad (\text{B3})$$

Thus, apparent stress drop is proportional to the static stress drop.

Finally, using the expression for σ_a (eq. 5), and the definitions of moment (eq. 12) and strain energy change (eq. 13), we obtain (Singh & Ordaz 1994),

$$E_r = 0.466 \Delta W. \quad (\text{B4})$$

In conclusion, the radiated energy in Brune's model is roughly 50 per cent of the strain energy, the other 50 per cent goes into rupture energy.